IEEE Access
Multidisciplinary | Rapid Review | Open Access Journal

Received 28 August 2023, accepted 6 September 2023, date of publication 13 September 2023,
date of current version 20 September 2023.

Digital Object Identifier 10.1109/ACCESS.2023.3314976

RESEARCH ARTICLE

Sparse Reconstruction-Based Time-Delay Estimation Algorithm in the Exponential Correlation Domain

LIN-FENG ZOU[1], YUN-FENG ZHU[1], JIE GU[2], JING-FEI JIANG[2], AND LU ZHANG[1]
[1]School of Mathematics, Sichuan University, Chengdu 610065, China
[2]National Key Laboratory of Electromagnetic Space Security, The 29th Research Institute of China Electronics Technology Group Corporation, Chengdu 610036, China

Corresponding author: Lu Zhang (zhanglumail@163.com)

ABSTRACT For the estimation problem of multiple adjacent targets, the traditional correlation function estimation method based on the matched filter (MF) is often limited by resolution, resulting in insufficient estimation accuracy. Subsequently, an exponential filter (EF) with high resolution was constructed by introducing a controllable exponent p into the frequency response function of the matched filter. In this paper, we propose a sparse reconstruction and exponential filter-based estimation algorithm to estimate the time delays of multiple targets. This algorithm uses the exponential autocorrelation function (the output of the exponential filter) as a template and constructs a sparse overcomplete model of the time delays of the received signal in the exponential correlation domain. An interior-point method based on l_1-norm regularization is then employed to solve the proposed overcomplete model. Notably, the proposed algorithm does not require prior knowledge of the target number. Theoretical analysis and Simulation results demonstrate that, the proposed algorithm can effectively reduce the coherence between adjacent targets and thus achieve high-accuracy time-delay estimation. When the input SNR is higher than -24 dB, it has a higher estimation accuracy for multi-target time delays (especially for adjacent targets) than the previous MF or EF based time-delay estimation algorithms. Particularly, at high signal-to-noise ratios, the estimation error of the proposed algorithm can approach the error bound of the time delays derived from the Cramér–Rao lower bound; when the input SNR is higher than -4 dB, it achieves completely accurate estimation.

INDEX TERMS Sparse reconstruction, compressive sensing, time-delay estimation, exponential filter, cross-correlation, l_1-norm regularization.

I. INTRODUCTION

Time delay estimation is critical in various domains, such as radar detection [1], sonar positioning [2], wireless communication [3], satellite communication [4], electronic equipment and materials [5], and so on. Moreover, it has emerged as a crucial area of research in related fields owing to the challenges posed by complex environments in multi-target time-delay estimation. The most traditional and effective algorithm for time-delay estimation is the correlation function-based algorithm, which utilizes a renowned matched filter (MF) [6], [7], [8], [9]. This class of algorithms has the advantages of low computational complexity and high output signal-to-noise ratios (SNRs). However, its target resolution is constrained [6], [8], and the output (i.e., the correlation function) often exhibits a broad main peak and high sidelobes, which can lead to peak overlap and large targets occluding small targets when adjacent multiple targets are present, resulting in inaccurate estimates of multi-target time delays.

With the continuous advancement of information technology and the increasing demand for accuracy in time-delay estimation, new theories and algorithms are continuously being applied to multi-target time-delay estimation problems in different environments with ideal

The associate editor coordinating the review of this manuscript and approving it for publication was Huaqing Li.

effects [10], [11], [12], [13], [14], [15], [16], [17]. Among them, the more traditional methods are the maximum likelihood estimation method [11] and subspace algorithm [13], [16]. As a theoretically optimal method, maximum likelihood estimation can approach the Cramér–Rao lower bound (CRLB) in high signal-to-noise ratio (SNR) environments. Nevertheless, this method has high computational complexity owing to the grid search process. Subspace algorithms are based on array signal processing that decomposes the receiving signal space into two orthogonal subspaces: a signal subspace and a noise subspace. In the case of multiple snapshots, high-precision multi-target time-delay estimates can be obtained by searching for pseudo-spectral peaks. However, under the conditions of a single snapshot and a low SNR, the performance of the subspace algorithm deteriorates significantly. Therefore, some researchers have proposed improved algorithms based on the modified correlation function method. For example, in [17], an exponential filter (EF) with a high resolution was constructed by introducing a controllable exponent p in the frequency response function of the MF. However, as a mismatched filter, the improvement in the resolution of EF still occurs at the expense of a loss in the output SNR.

Furthermore, compressed sensing, an emerging theory at the intersection of signal processing and optimization, has attracted significant attention from both academia and industry over the past decade and has been successfully applied in many fields, such as signal processing [18], image science [19], machine learning [20], statistical modeling [21] and medical data analysis [22]. Recently, scholars have applied the principle of sparse reconstruction (SR) in compressive sensing for time-delay estimation. Reference [23] constructed an SR model of time delays of the received signal in the frequency domain and then used the orthogonal matching pursuit (OMP) algorithm to solve the multi-target time-delay estimation problem under the assumption of knowing the number of targets. However, with an increase in the discrete time-delay grid points, the mutual coherence of the column vectors in the observation matrix also increases, making it prone to finding suboptimal solutions. Hence, based on the SR model in the frequency domain, a backtracking selection mechanism using the OMP algorithm was proposed to provide an unbiased estimate of multi-target time delays [24]. However, this algorithm increases the computational complexity to achieve an improved resolution. It also requires the knowledge of the number of targets. Subsequently, SR- and MF-based time-delay estimation algorithms were constructed for linear frequency-modulated (LFM) signals [25]. The algorithm uses the output of the MF (i.e., the autocorrelation function) as a template to construct the SR model (in the correlation domain) for the time delays of multiple targets, and it can accurately estimate multi-target time delays with an available number of targets and a high input SNR. However, its output resolution is also limited owing to the use of MF, and introducing covariance matrix iterative computation also increases computational complexity.

Classic time-delay estimation methods based on correlation function are often limited in time-delay estimation accuracy by their target resolution. Inspired by the high resolution of multiple targets of EF, in this study, an SR-based estimation algorithm in the exponential correlation domain is constructed for the estimation of time delays of multiple targets, in which the SR model is constructed using the output of the EF (i.e., the exponential autocorrelation function) as a template. The interior-point method [26] based on l_1-norm regularization, was employed to solve the proposed SR model without knowing the number of targets in advance. Through derivation and verification, it is shown that owing to the high resolution of the output of EF, the corresponding observation matrix of the proposed SR model in the exponential correlation domain has a smaller partial mutual coherence coefficient than that of the SR model in the correlation domain, thus providing a higher reconstruction performance for delays in adjacent targets. However, because EF is mismatched, noise still affects its output. The traditional wavelet denoising algorithm [27], [28], which is a highly effective nonlinear denoising algorithm, has been successfully applied to signal processing in various practical scenarios and can effectively remove noise from smooth signals. Therefore, this study preprocesses the EF output using the wavelet denoising algorithm.

Based on simulation experiments, where LFM signals are used as the reference signal, this study shows that when the input SNR is higher than -24 dB, the proposed SR-based estimation algorithm in the exponential correlation domain (SR-ECD) for multi-target time delay estimation outperforms the traditional estimation algorithms based on the correlation function or exponential correlation function, and the SR-based estimation algorithm in the correlation domain (SR-CD). The proposed SR-ECD algorithm provides a higher resolution for adjacent targets and significantly lower estimation errors in multi-target time-delay estimation. Moreover, the estimation errors obtained by SR-ECD are closer to the error bound derived from the CRLB of the multi-target time-delay estimation.

Thus, the proposed algorithm can effectively reduce the coherence between adjacent targets and thus achieve high-accuracy of time-delay estimation under the condition of a low input signal-to-noise ratio. Moreover, it does not require prior knowledge of the number of targets and is suitable for high-dimensional data scenarios.

II. EXPONENTIAL CORRELATION FUNCTION

Assuming that the reference signal emitted by the radiation source is $r(t)$, the noisy received signal containing K targets can be represented as:

$$x(t) = \sum_{i=1}^{K} a_i r(t - \tau_i) + n(t), \tag{1}$$

where a_i and τ_i represent the amplitude and time-delay of the i-th target, respectively, $i = 1,2,\ldots, K$, and the additive noise $n(t)$ is a zero-mean Gaussian white noise with variance σ^2.

The correlation function-based time-delay estimation method using MF [6] obtains the estimated time delays of multiple targets by searching for the peak values of the MF output (i.e., the cross-correlation function between the reference signal $r(t)$ and the received signal $x(t)$).

Introducing a controllable exponent $p \in [-1, 1]$ in the frequency response function of the MF yields the frequency response function of EF [17]

$$H_p(\omega) = |R(\omega)|^{1+p} R^{-1}(\omega), \tag{2}$$

where $R(\omega)$ denotes the Fourier transform of $r(t)$. The impulse response function $h_p(t)$ of EF is the inverse Fourier transform of $H_p(\omega)$. The output of the reference signal $r(t)$ through the EF is called the **exponential autocorrelation function** of $r(t)$, and is denoted as

$$r_p(t) = r * h_p(t), \tag{3}$$

where $*$ represents the convolution operation. The output of the received signal $x(t)$ through the EF is called the p-order **exponential cross-correlation function** of $r\,(t)$and $x(t)$, denoted as $x_p(t) = x * h_p(t)$, which is the output of the received signal in the p-order exponential correlation domain.

Evidently, when $p = 1$, EF is reduced to the classic MF. It was rigorously proven in [17] that for any $p \in [-1, 1]$, the p-order exponential cross-correlation function of the received signal reaches its extreme values at the target delays, and the exponential cross-correlation function with $p < 1$ has a higher resolution than the classic cross-correlation function ($p = 1$). Generally, the smaller the exponent p, the greater the resolution of the output in the exponential correlation domain, but the lower the output SNR.

It can be seen that the resolution and output SNR of the received signal in the exponential correlation domain are both determined by exponent p and there exists an inherent trade-off between them. Therefore, the selection of the optimal exponent in different signal environments is particularly important, and often needs to follow a compromise criterion. This study used the method proposed in Ref. [17] to determine the optimal exponent p_{opt}, that is, to maximize the multi-target resolution $ISL(p)$ under the premise that the output signal-to-noise ratio $SNR(p)$ of the received signal is greater than a pre-determined SNR threshold S_0:

$$p_{opt} = arg \max_{p\in[-1,1]} ISL(p), \quad s.t.\ SNR(p) \geq S_0, \tag{4}$$

where $ISL(p)$ and $SNR(p)$ represent the target resolution and SNR of the output of p-order EF, given by the following equations:

$$\mathrm{ISL}\,(p) = 10\lg \frac{\int_{-\infty}^{+\infty} \left|r_p\,(t)\right|^2 dt}{\left|r_p\,(0)\right|^2},$$

$$\mathrm{SNR}(p) = 10\lg \frac{\left|r_p(0)\right|^2}{\sigma \int_{-B}^{+B} \left|H_p(\omega)\right|^2 d\omega}.$$

III. SR-BASED TIME-DELAY ESTIMATION ALGORITHM IN THE EXPONENTIAL CORRELATION DOMAIN

A. SR MODEL IN THE EXPONENTIAL CORRELATION DOMAIN FOR TIME-DELAY ESTIMATION

Assume that the discrete sampling signal of $r(t)$ is $r[m] = r(m\Delta t), m = 1, 2, \ldots, M$, with a sampling interval of Δt. According to the pre-determined output SNR threshold S_0 and the optimal exponent selection criterion (4) given in Sect. II, EF with the optimal exponent $p$is obtained and denoted as H_p. The frequency response function, $H_p(\omega)$ is given by the discrete form of (2). The discrete form of the exponential autocorrelation function was obtained by inputting a discrete reference signal to H_p:

$$\begin{aligned} r_p[m] &= r * h_p[m] \\ &= \sum_{n=1}^{M} r[m-n]h_p[n], \quad m = 1, \ldots, M. \end{aligned} \tag{5}$$

Assume that the time-delay τ_i of the i-th target is at the sampling point, i.e., $\tau_i = d_i\Delta t, i = 1, 2, \ldots, K$, where d_i is an integer between 1 and M, the discrete form of the received signal $x(t)$ in (1) can be written as

$$x[m] = \sum_{i=1}^{K} a_i r[m - d_i] + n[m], \quad m = 1, 2, \ldots, M. \tag{6}$$

The discrete form of the exponential cross-correlation function is obtained by inputting the $x[m]$ in (6) into H_p as follows:

$$x_p\,[m] = x * h_p\,[m] = \sum_{i=1}^{K} a_i r_p\,[m - d_i] + n_p\,[m], \tag{7}$$

$m= 1, 2, \ldots, M$. Here, $n_p[m] = n * h_p[m]$ is the discrete output of the noise $n(t)$ of H_p, and r_p is the discrete exponential cross-correlation function of $r\,(t)$given by (3).

To further eliminate the output noise of the EF, we use the classical wavelet soft-thresholding filtering algorithm [27] to denoise its output, and the result is denoted as $\tilde{x}_p[m]$. The noise after the wavelet processing is denoted as $\tilde{n}_p[m]$. Therefore, the denoised exponential cross-correlation function can be rewritten as

$$\tilde{x}_p\,[m] = \sum_{i=1}^{K} a_i r_p\,[m - d_i] + \tilde{n}_p\,[m], \quad m = 1, 2, \ldots, M. \tag{8}$$

The above equation can be rewritten as the following linear observation model:

$$\boldsymbol{y}_p = \boldsymbol{A}_p\boldsymbol{a} + \boldsymbol{w}_p, \tag{9}$$

where $\boldsymbol{y}_p = \left[\tilde{x}_p[1], \tilde{x}_p[2], \ldots, \tilde{x}_p[M]\right]^T$ is the observation vector, $\boldsymbol{a} = [a_1, a_2, \ldots, a_K]^T$ is the target amplitude vector, the noise vector is $\boldsymbol{w}_p = \left[\tilde{n}_p[1], \tilde{n}_p[2], \ldots, \tilde{n}_p[M]\right]^T$. Here T represents transpose, and the observation matrix is

$$\boldsymbol{A}_p = \begin{bmatrix} r_p[1-d_1] & r_p[1-d_2] & \ldots & r_p[1-d_K] \\ r_p[2-d_1] & r_p[2-d_2] & \ldots & r_p[2-d_K] \\ & & & \\ r_p[M-d_1] & r_p[M-d_2] & \ldots & r_p[M-d_K] \end{bmatrix}_{M\times K}. \tag{10}$$

The above linear observation model was not sparse. To extend it to an overcomplete sparse form, we set up a N dimensional discrete delay grid $\bar{\boldsymbol{d}} = \left[\bar{d}_1, \bar{d}_2, \ldots, \bar{d}_N\right]$ in a certain delay range (T_a, T_b), $\bar{d}_i$ is an integer and $i = 1, \ldots, N$. We assume that all discrete values of the target time delay are in the grid, that is, $\tau_i \in T_a + \bar{\boldsymbol{d}}\,(T_b - T_a)/N$. Let the zeropadding extended form of the target amplitude vector be $\bar{\boldsymbol{a}} = [\bar{a}_1, \bar{a}_2, \ldots, \bar{a}_N]^T$, and $\bar{\boldsymbol{a}}$ have nonzero components $\bar{a}_i = a_i$ (the true amplitude of the target) if and only if $T_a + \bar{d}_i\,(T_b - T_a)/N = \tau_i = d_i \Delta t$ (the true discrete values of the target delay); otherwise, $\bar{a}_i = 0$. When the total number of grids N is much larger than the true number of targets K, $\bar{\boldsymbol{a}}$ is a K snarse N-dimensional vector

Meanwhile, the extended form of observation matrix $\boldsymbol{A}_p$ is denoted as

$$\bar{A}_p = \begin{bmatrix} r_p\left[1-\bar{d}_1\right] & r_p\left[1-\bar{d}_2\right] & \ldots & r_p\left[1-\bar{d}_N\right] \\ r_p\left[2-\bar{d}_1\right] & r_p\left[2-\bar{d}_2\right] & \ldots & r_p\left[2-\bar{d}_N\right] \\ & & & \\ r_p\left[M-\bar{d}_1\right] & r_p\left[M-\bar{d}_2\right] & \ldots & r_p\left[M-\bar{d}_N\right] \end{bmatrix}_{M\times N} \tag{11}$$

In conclusion, we obtain the (overcomplete) SR model of the multi-target time-delay estimation problem in the exponential correlation domain:

$$y_p = \bar{A}_p \bar{\boldsymbol{a}} + \boldsymbol{w_p}. \tag{12}$$

Our goal is to find the sparse vector $\bar{\boldsymbol{a}}$, where the locations of its nonzero components represent the estimated values of the time delays.

B. THE ALGORITHM FOR SOLVING THE SR MODEL IN THE EXPONENTIAL CORRELATION DOMAIN

In this section, we consider using an interior-point method [26] based on l_1-norm regularization to solve the exponential domain SR model (12), which does not require knowledge of the number of targets. In fact, (12) can be transformed into an l_1-norm regularized model:

$$\widehat{\boldsymbol{a}} = \underset{\bar{\boldsymbol{a}}}{\operatorname{argmin}} \left\|\boldsymbol{y}_p - \bar{A}_p \bar{\boldsymbol{a}}\right\|_2^2 + \lambda \|\bar{\boldsymbol{a}}\|_1, \tag{13}$$

where $\|\bullet\|_1$, $\|\bullet\|_2$ denote the l_1 and l_2 norms of the vector, respectively, and λ represents the hyperparameter.

The interior-point method first transforms regularized model (13) into a convex quadratic optimization problem with linear inequality constraints:

$$\begin{aligned} \widehat{\boldsymbol{a}} = \underset{\bar{\boldsymbol{a}}}{\operatorname{argmin}} \left\|\bar{\boldsymbol{A}}_{\boldsymbol{p}} \bar{\boldsymbol{a}} - \boldsymbol{y_p}\right\|_2^2 + \lambda \sum_{n=1}^{N} u_n, \\ \text{s.t. } -u_n \le \bar{a}_n \le u_n, \quad n = 1, \ldots, N, \end{aligned} \tag{14}$$

where u_n represents the constraint boundary for the nth component $\bar{a}_i$ of the target amplitude vector $\bar{\boldsymbol{a}}$. Let iteration vector $\boldsymbol{u} = [u_1, \ldots, u_N]^T \in R^N$.

Starting from the initial values of $\bar{\boldsymbol{a}} = [0, \ldots, 0]^T \in R^N$, $t = 1/\lambda$, and $\boldsymbol{u} = [1, \ldots, 1]^T \in R^N$, the iteration process is used to approach an approximate solution $\hat{\boldsymbol{a}}$ to model (14) using a sequence of iterations for $\bar{\boldsymbol{a}}$. The iterative steps for the approximation are as follows:

A1: The preconditioned conjugate gradient (PCG) algorithm was used to obtain the iterative direction vectors $\Delta \boldsymbol{a}$and $\Delta \boldsymbol{u}$ for $\bar{\boldsymbol{a}}$ and $\boldsymbol{u}$ at each step:

$$\begin{bmatrix} 2\,t\bar{\boldsymbol{A}}_p^T \bar{\boldsymbol{A}}_p + \boldsymbol{D}_1 & \boldsymbol{D}_2 \\ \boldsymbol{D}_2 & \boldsymbol{D}_1 \end{bmatrix} \begin{bmatrix} \Delta \boldsymbol{a} \\ \Delta \boldsymbol{u} \end{bmatrix} = - \begin{bmatrix} \boldsymbol{g}_1 \\ \boldsymbol{g}_2 \end{bmatrix}$$

where the intermediate variables $\boldsymbol{D}_1, \boldsymbol{D}_2, \boldsymbol{g}_1, \boldsymbol{g}_2$ are given in Ref. [26].

A2: Compute the value of $s = \beta^\rho$ to obtain the step size for each iteration, where α and β represent predefined constants, and ρ represents the smallest positive integer satisfying the following inequality:

$$\phi_t\left(\bar{\boldsymbol{a}} + \beta^\rho \Delta \boldsymbol{a}, \boldsymbol{u} + \beta^\rho \Delta \boldsymbol{u}\right) \le \phi_t(\bar{\boldsymbol{a}}, \boldsymbol{u}) + \alpha \beta^\rho \begin{bmatrix} \boldsymbol{g_1} \\ \boldsymbol{g_2} \end{bmatrix}^T \begin{bmatrix} \boldsymbol{\Delta a} \\ \boldsymbol{\Delta u} \end{bmatrix},$$

here,

$$\begin{aligned} \phi_t(\bar{\boldsymbol{a}}, \boldsymbol{u}) = t \left\|\bar{\boldsymbol{A}}_p \bar{\boldsymbol{a}} - \boldsymbol{y_p}\right\|_2^2 + t \sum\nolimits_{n=1}^{N} \lambda u_n - \sum\nolimits_{n=1}^{N} \lg\left(u_n \right. \\ \left. + \bar{a}_n\right) - \sum\nolimits_{n=1}^{N} \lg\left(u_n - \bar{a}_n\right). \end{aligned}$$

A3: Update $\bar{\boldsymbol{a}}$ and $\boldsymbol{u}$ based on one iteration of the calculation using s and $\begin{bmatrix} \Delta \boldsymbol{a} & \Delta \boldsymbol{u} \end{bmatrix}^T$ as follows:

$$\begin{bmatrix} \bar{\boldsymbol{a}} \\ \boldsymbol{u} \end{bmatrix} = \begin{bmatrix} \bar{\boldsymbol{a}} \\ \boldsymbol{u} \end{bmatrix} + s \begin{bmatrix} \Delta \boldsymbol{\alpha} \\ \Delta \boldsymbol{u} \end{bmatrix}.$$

A4: If the iterative error ξ is less than the preset threshold ε_{rel}, the approximate solution $\hat{\boldsymbol{a}} = \bar{\boldsymbol{a}}$. If ξ is greater than or equal to ε_{rel}, t is updated according to the following formula, and returns to step A1 to continue the calculation iteration:

$$t := \begin{cases} \max\left\{\mu \min\left\{2N/\eta, t\right\}, t\right\} & s \ge s_{\min} \\ t & s < s_{\min}, \end{cases}$$

where μ and $s_{\min}$ are pre-set hyperparameters, and η is given in [26].

C. ALGORITHM FLOW OF THE SR-BASED ESTIMATION ALGORITHM IN THE EXPONENTIAL CORRELATION DOMAIN

The basic procedure of SR-ECD proposed in this paper for multi-target time-delay estimation is as follows:

Step 1: Based on the reference signal $r(t)$, we use the optimal exponent selection method in Section. II.B to select the optimal exponent p, and construct EF denoted as H_p, with the frequency response function $H_p(\omega) = |R(\omega)|^{1+p} R^{-1}(\omega)$. The output of $r(t)$through H_p is the exponential autocorrelation function $r_p(t)$.

Step 2: Input the received signal $x(t)$ into H_p to obtain the exponential cross-correlation function in the domain.

Step 3: The wavelet soft thresholding algorithm is applied to denoise the aforementioned exponential cross-correlation function.

Step 4: Construct the SR model of the multi-target time-delay estimation problem in the exponential correlation domain according to (12).

Step 5: Solve the SR model using the interior-point method to obtain the estimation values of the multi-target time delays.

IV. PERFORMANCE ANALYSIS OF THE PROPOSED ALGORITHM

In this section, we provide an analysis of reconstructing performance of the SR-ECD proposed for multi-target time-delay estimation, by analyzing the mutual coherence of the observation matrix of the SR model (12) in the exponential correlation domain, and as we will show, using the exponential autocorrelation function as the template for the SR model can make the corresponding observation matrix have a smaller partial mutual coherence coefficient, thus providing a higher reconstructing performance of delays of adjacent targets. We also derive the error bound of the time-delay estimation error in the multi-target case based on the CRLB.

A. ANALYSIS OF MUTUAL COHERENCE OF THE OBSERVATION MATRIX IN THE SR MODEL

For the SR model (12), whether the observation $\boldsymbol{y}_p$ contains sufficient information to recover the sparse vector $\bar{\boldsymbol{a}}$ depends mainly on the properties of the observation matrix $\bar{A}_p$. Generally, the observation matrix must satisfy properties such as Spark, Null Space Property (NSP), or Restricted Isometry Property (RIP) to guarantee the success of SR methods for reconstructing sparse vectors [29]. Current research shows that as long as the observation matrix satisfies the Kth-order RIP property, a K-sparse vector can be reconstructed from M observations. Although RIP has perfect properties, verifying that the RIP criterion is a combinatorial problem, so it is more practical to verify that the observation matrix has equivalent condition requirements, such as the mutual coherence condition [30]. Definition 1 provides the definition of the mutual coherence coefficient.

Definition 1 [31]: Given a matrix $\boldsymbol{A}$ of size $M \times N$, the mutual coherence coefficient $\mu(\boldsymbol{A})$ is defined as the maximum absolute value of the inner product between any two normalized columns of $\boldsymbol{A}$, that is,

$$\mu(\boldsymbol{A}) = \max_{k,l=1,\ldots,N,,k\neq l} \frac{\left|\boldsymbol{a}_k^H \boldsymbol{a}_l\right|}{\|\boldsymbol{a}_k\|_2 \|\boldsymbol{a}_l\|_2}. \tag{15}$$

From the definition of mutual coherence, it can be seen that the calculation of $\mu(\boldsymbol{A})$ is easy to implement, and this metric reflects the reconstruction performance of sparse vectors by overcomplete model (12). Regarding the mutual coherence coefficient, the following conclusion can be drawn.

Theorem 1 [31]: Suppose that the mutual coherence coefficient of matrix $\boldsymbol{A}$ is μ, and $\boldsymbol{x}$ is a K-sparse vector, $K < (1/\mu + 1)/4$. Let the observations be obtained as $\boldsymbol{y} = \boldsymbol{A}\boldsymbol{x} + \boldsymbol{e}$. Then, for $B(\boldsymbol{y}) = \left\{\boldsymbol{w} : \|\boldsymbol{A}\boldsymbol{w} - \boldsymbol{y}\|_2 \leq \varepsilon\right\}$, the solution $\hat{\boldsymbol{x}}$ of model $\hat{\boldsymbol{x}} = \underset{\boldsymbol{w}\in B(\boldsymbol{y})}{\operatorname{argmin}} \|\boldsymbol{w}\|_1$ satisfies:

$$\left\|\boldsymbol{x} - \hat{\boldsymbol{x}}\right\|_2 \leq \frac{\|\boldsymbol{e}\|_2 + \varepsilon}{\sqrt{1 - \mu(4K-1)}}. \tag{16}$$

From Definition 1 and Theorem 1, it can be seen that as the mutual coherence coefficient μ of the observation matrix decreases, the non-coherence between the column vectors of the observation matrix becomes stronger, the upper bound of the reconstruction error for sparse vectors becomes smaller, and the reconstruction ability of the original signal increases. On the other hand, as the μ decreases, the right-hand side of the inequality $K < (1/\mu + 1)/4$ in Theorem 1 increases, which increases the upper bound of K and reduces the sparsity requirement for the $\boldsymbol{x}$. Donoho et al. pointed out that Theorem 1 is an analysis result under the worst-case scenario, the reconstruction error $\left\|\boldsymbol{x} - \hat{x}\right\|_2$ is estimated to be too large, and the actual error in practical applications is generally much smaller than the estimated value in the theorem.

In this study, we derive that for the SR model (12) of the received signal in the exponential correlation domain, the partial mutual coherence coefficient of the observation matrix (i.e., the mutual coherence coefficient of its M-dimensional sub-matrix) decreases as exponent p decreases. Consequently, the sparsity requirement and upper bound of the reconstruction error for the corresponding time-delay vector also decrease. In other words, we conclude the following.

Theorem 2: For the SR model (12) with observation matrix $\bar{\boldsymbol{A}}_p$, the mutual coherence coefficient of any specified submatrix consisting of M column vectors is defined as its partial mutual coherence coefficient $\tilde{\mu}\left(\overline{\boldsymbol{A}}_p\right)$. Then, there exists a real number $\delta_Z \in (-1, 1)$ such that when $p \in [-1, \delta_Z]$, $\tilde{\mu}\left(\overline{\boldsymbol{A}}_p\right)$

Proof: The observation matrix $\overline{\boldsymbol{A}}_p$ of the SR model (12) can be regarded as obtained by selecting a specified M row from cyclic matrix $\overline{\overline{\boldsymbol{A}}}_p$, where

$$\overline{\overline{\boldsymbol{A}}}_p = \begin{bmatrix} r_p\left[\bar{d}_1\right] & r_p\left[\bar{d}_2\right] & \cdots & r_p\left[\bar{d}_N\right] \\ r_p\left[\bar{d}_2\right] & r_p\left[\bar{d}_3\right] & \cdots & r_p\left[\bar{d}_1\right] \\ & & & \\ r_p\left[\bar{d}_N\right] & r_p\left[\bar{d}_1\right] & \cdots & r_p\left[\bar{d}_{N-1}\right] \end{bmatrix}_{N\times N}$$

Based on linear algebra and the construction method of exponential correlation functions, the cyclic matrix $\overline{\overline{\boldsymbol{A}}}_p$ can be represented as

$$\overline{\overline{\boldsymbol{A}}}_p = \frac{1}{N}\boldsymbol{F} \cdot \operatorname{diag}[z_1^{p+1}, \cdots, z_N^{p+1}] \cdot \boldsymbol{F}^H,$$

where $\boldsymbol{F}$ is the $N \times N$ Fourier matrix, with its k-th row and l-th column element being $\exp[-j2\pi\,(k-1)\,(l-1)\,/N]$, and $j = \sqrt{-1}$ is the imaginary unit. Let $\boldsymbol{f}_1, \ldots, \boldsymbol{f}_N$ be the row vector of $\boldsymbol{F}$, and $z_i = |g_i|$ $(i = 1, 2, \ldots, N)$ be the absolute value of the Fourier frequency coefficient, i.e., $\left[g_1 \cdots g_N\right]^T = \boldsymbol{F}\left[r\left[\bar{d}_1\right], \cdots, r[\bar{d}_N]\right]^T$.

Obviously, $z_i > 0, i = 1, 2, \ldots, N$. Without loss of generality, assume that the mean value of $z_1, \ldots, z_N$ is 1; otherwise, the reference signal can be simply divided by its mean. Therefore, $\overline{\overline{\boldsymbol{A}}}_p$ can be rewritten as

$$\overline{\overline{\boldsymbol{A}}}_p = \frac{1}{N}\boldsymbol{F}\boldsymbol{Z}\boldsymbol{F}^H + \boldsymbol{I}_{N\times N},$$

where $\boldsymbol{I}_{N\times N}$ is the N-dimensional identity matrix, $\boldsymbol{Z} = \mathrm{diag}[z_1^{p+1} - 1, \cdots, z_N^{p+1} - 1]$ is a diagonal matrix.

Let $\overline{\boldsymbol{A}}_p$ be the submatrix obtained by selecting the $N_1, N_2, \ldots, N_M$ rows of $\overline{\overline{\boldsymbol{A}}}_p$, and the i-th column vector of $\overline{\boldsymbol{A}}_p$ be $\boldsymbol{a}_{p(i)}, i = 1, \ldots, N$. Now we consider the partial mutual coherence coefficient of $\overline{\boldsymbol{A}}_p$, that is, the maximum absolute value of the cosine of the angle between the $N_1, N_2, \ldots, N_M$ columns of $\overline{\boldsymbol{A}}_p$:

$$\tilde{\mu}(\overline{\boldsymbol{A}}_p) = \max_{k\neq l(k,l=1,\ldots,M)} \frac{\left|\boldsymbol{a}_{p(N_k)}^H \boldsymbol{a}_{p(N_l)}\right|}{\left\|\boldsymbol{a}_{p(N_k)}\right\|_2 \left\|\boldsymbol{a}_{p(N_l)}\right\|_2}. \tag{17}$$

As the structure of $\overline{\boldsymbol{A}}_p$ implies that $\boldsymbol{a}_{p(N_k)} = \boldsymbol{z}_{p(N_k)} + \boldsymbol{\varepsilon}_{N_k}$ for any $k = 1, 2, \ldots, M$, where $\boldsymbol{\varepsilon}_{N_k}$ is an M-dimensional unit column vector with the N_k-th element being 1 and all others being 0, $\boldsymbol{z}_{p(N_k)}$ is given by the following equation:

$$\boldsymbol{z}_{p(N_k)} = \frac{1}{N}\left[\boldsymbol{f}_{N_1}, \ldots, \boldsymbol{f}_{N_M}\right]^T \boldsymbol{Z} \cdot \boldsymbol{f}_{N_k}^H.$$

As $\boldsymbol{F}/\sqrt{N}$ is a unitary matrix, it follows that the l_2 norms of any row and any column of $\boldsymbol{F}/\sqrt{N}$ are both equal to 1, so we have

$$\left\|\boldsymbol{z}_{p(N_k)}\right\|_2 \leq Z_{\max} \overset{\text{def}}{=} \max\left\{\left|z_1^{p+1} - 1\right|, \ldots, \left|z_N^{p+1} - 1\right|\right\}.$$

For a fixed $z_1, z_2, \ldots, z_N$, $Z_{\max}$ is a continuous function with respect to p. And in the EF, as p decreases, $Z_{\max}$ monotonically decreases. Moreover, when the exponent $p \to -1$, then $Z_{\max} \to 0$. Therefore, there exists a $\delta_{\boldsymbol{Z}} \in (-1, 1)$, when $p \in [-1, \delta_{\boldsymbol{Z}}]$, then $0 \leq Z_{\max} < 1$.

Therefore, when $p\,[-1, \delta_Z]$, the partial mutual coherence coefficient $\tilde{\mu}\left(\overline{\boldsymbol{A}}_p\right)$satisfies the following constraints according to the Schwarz inequality:

$$\begin{aligned}\tilde{\mu}\left(\overline{\boldsymbol{A}}_p\right) &= \max_{k\neq l(k,l=1,\ldots,M)} \frac{\left|\boldsymbol{a}_{p(N_k)}^H \boldsymbol{a}_{p(N_l)}\right|}{\left\|\boldsymbol{a}_{p(N_k)}\right\|_2 \left\|\boldsymbol{a}_{p(N_l)}\right\|_2} \\ &= \max_{k\neq l(k,l=1,\ldots,M)} \frac{\left|\left(\boldsymbol{z}_{p(N_k)} + \boldsymbol{\varepsilon}_{N_k}\right)^H \left(\boldsymbol{z}_{p(N_l)} + \boldsymbol{\varepsilon}_{N_l}\right)\right|}{\left\|\boldsymbol{a}_{p(N_k)}\right\|_2 \left\|\boldsymbol{a}_{p(N_l)}\right\|_2} \\ &\leq \frac{2Z_{\max} + Z_{\max}^2}{|1 - Z_{\max}|^2} \overset{\text{def}}{=} Y\left(Z_{\max}\right).\end{aligned}$$

According to the derivative of $Y(Z_{\max})$ with respect to $Z_{\max}$, it can be seen that $Y(Z_{\max})$ monotonically decreased to 0 as $Z_{\max}$ decreased.

The above derivation shows that when exponent $p \in [-1, \delta_Z]$, the upper bound $Y(Z_{\max})$ of the partial mutual coherence coefficient $\tilde{\mu}(\overline{\boldsymbol{A}}_p)$ monotonically decreases to 0 as exponent p decreases. It can be seen that the smaller the exponent p, the closer matrix $\boldsymbol{Z}$ is to the zero matrix ($\boldsymbol{Z} \to \boldsymbol{0}_{N\times N}$ when $p \to -1$), the more dominant the diagonal of the cyclic matrix $\overline{\overline{\boldsymbol{A}}}_p$, and the more the adjacent columns of $\overline{\overline{\boldsymbol{A}}}_p$ are orthogonal, the smaller the partial mutual coherence coefficient. □

We present the curve of the partial mutual coherence coefficient $\tilde{\mu}(\overline{\boldsymbol{A}}_p)$ of the observation matrix $\overline{\boldsymbol{A}}_p$ with respect to exponent p by numerical simulations. In the simulations, the reference signal $r(t)$ was chosen as an LFM signal with a bandwidth of 10 MHz and starting carrier frequency of 3000 kHz, and the sampling size was $M = 100$ with a grid number of $N = 200$. We constructed corresponding observation matrices for different p values and calculated their partial mutual coherence coefficients. As shown in Figure 1, the partial mutual coherence coefficient shows a decreasing trend as exponent p decreases, which is in complete agreement with the conclusion of Theorem 2 that we derived. In particular, when p decreased to a certain range, the partial mutual coherence coefficient decreased significantly. Specifically, when $p = 1$, the partial mutual coherence coefficient $\tilde{\mu}(\overline{\boldsymbol{A}}_p)$ is the partial mutual coherence coefficient of the observation matrix of SR-CD.

In summary, the observation matrix of the proposed SR-ECD in this study has a lower partial mutual coherence than the observation matrix of the SR-CD based on traditional MF. Therefore, for adjacent targets, the reconstruction performance of SR-ECD in the exponential correlation domain was better than that of SR-CD. Moreover, the lower the value of p, the higher the reconstruction performance for multiple target time delays.

B. THE ERROR LOWER BOUND FOR MULTI-TARGET TIME-DELAY ESTIMATION

The received signal in the time domain for multi-target is given by (6), and its discrete Fourier transform is:

$$\hat{X}\left(m\Delta\omega\right) = \sum_{i=1}^{K} a_i R\left(m\Delta\omega\right) e^{-j\tau_i m\Delta\omega} + \hat{N}\left(m\Delta\omega\right), \tag{18}$$

$m = 1, 2, \ldots, M$. Here, let $\hat{X}(\omega), R(\omega)$ and $\hat{N}(\omega)$ be the Fourier transforms of received signal $x(t)$, the reference signal $r(t)$, and the noise $n(t)$, respectively. Denote $\hat{X}(m\Delta\omega) = X[m], \hat{N}(m\Delta\omega) = N[m], m = 1, 2, \ldots, M$, then Eq.(18) can be written as

$$\boldsymbol{S} = \boldsymbol{A}\left(\boldsymbol{\tau}\right)\boldsymbol{a} + \boldsymbol{N}, \tag{19}$$

where the observation vector, target amplitude vector, and noise vector are $\boldsymbol{S} = [X[1], X[2], \ldots, X[M]]^T, \boldsymbol{a} = [a_1, a_2, \ldots, a_K]^T, \boldsymbol{N} = [N[1], N[2], \ldots, N[M]]^T$, respectively.

The observation matrix as shown in the equation at the bottom of the next page.

Obviously, the matrix $\boldsymbol{A}\left(\boldsymbol{\tau}\right)\left[\boldsymbol{A}\left(\tau_1\right), \cdots, \boldsymbol{A}\left(\tau_K\right)\right]$ has more rows than columns ($M > K$) and the column vectors are linearly independent. $\boldsymbol{N}$ is a random vector with a Gaussian distribution and $E[\boldsymbol{N}\boldsymbol{N}^H] = M\sigma^2\boldsymbol{I}$. The log-likelihood

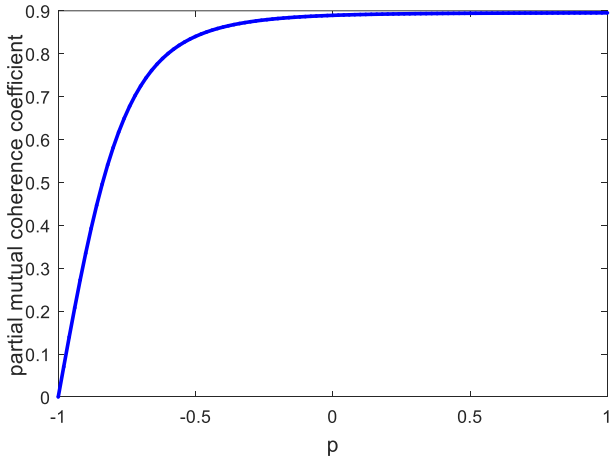

FIGURE 1. Partial mutual coherence of SR model (12) in the exponential correlation domain over exponent *p*.

function can be derived from Equation (19):

$$\ln L = \text{const} - 2M \ln \sigma - \frac{1}{M\sigma^2}[\boldsymbol{S}^H - \boldsymbol{a}^H \boldsymbol{A}^H(\boldsymbol{\tau})] \cdot [\boldsymbol{S} - \boldsymbol{A}(\boldsymbol{\tau})\boldsymbol{a}]. \quad (20)$$

Then, we derive the partial derivative of the log-likelihood function $ln\ L$ with respect to σ^2, $\mathrm{Re}(\boldsymbol{a})$ (i.e., the real part of $\boldsymbol{a}$), and $\mathrm{Im}(\boldsymbol{a})$(i.e., the imaginary part of $\boldsymbol{a}$), respectively:

$$\begin{aligned}
\frac{\partial \ln L}{\partial \sigma^2} &= -\frac{M}{\sigma^2} + \frac{M}{\sigma^4}\boldsymbol{N}^H\boldsymbol{N};\\
\frac{\partial \ln L}{\partial \mathrm{Re}(\boldsymbol{a})} &= \frac{1}{M\sigma^2}\left[\boldsymbol{A}^H(\boldsymbol{\tau})\boldsymbol{N} + \boldsymbol{A}^T(\boldsymbol{\tau})\boldsymbol{N}^H\right]\\
&= \frac{2}{M\sigma^2}\mathrm{Re}\left[\boldsymbol{A}^H(\boldsymbol{\tau})\boldsymbol{N}\right];\\
\frac{\partial \ln L}{\partial \mathrm{Im}(\boldsymbol{a})} &= \frac{1}{M\sigma^2}\left[-j\boldsymbol{A}^H(\boldsymbol{\tau})\boldsymbol{N} + j\boldsymbol{A}^T(\boldsymbol{\tau})\boldsymbol{N}^*\right]\\
&= \frac{2}{M\sigma^2}\mathrm{Im}\left[\boldsymbol{A}^H(\boldsymbol{\tau})\boldsymbol{N}\right];\\
\frac{\partial \ln L}{\partial \tau_k} &= \frac{2}{M\sigma^2}\mathrm{Re}\left[X^*[k]\boldsymbol{d}^H(\tau_k)\boldsymbol{N}\right].
\end{aligned}$$

Here, $\boldsymbol{d}(\tau_k) = d\boldsymbol{A}(\tau_k)/d\tau_k$. Because the knowledge of linear algebra, note that $E[\boldsymbol{N}\boldsymbol{N}^T] = \boldsymbol{0}$, further leads to

$$\begin{aligned}
E\left[\left(\frac{\partial \ln L}{\partial \mathrm{Im}(\boldsymbol{a})}\right)\left(\frac{\partial \ln L}{\partial \boldsymbol{\tau}}\right)^T\right] &= \frac{2}{M\sigma^2}\mathrm{Im}\left[\boldsymbol{A}^H(\boldsymbol{\tau})\boldsymbol{D}\boldsymbol{\alpha}\right],\\
E\left[\left(\frac{\partial \ln L}{\partial \mathrm{Re}(\boldsymbol{a})}\right)\left(\frac{\partial \ln L}{\partial \mathrm{Im}(\boldsymbol{a})}\right)^T\right] &= -\frac{2}{M\sigma^2}\mathrm{Im}\left[\boldsymbol{A}^H(\boldsymbol{\tau})\boldsymbol{A}(\boldsymbol{\tau})\right],\\
E\left[\left(\frac{\partial \ln L}{\partial \mathrm{Re}(\boldsymbol{a})}\right)\left(\frac{\partial \ln L}{\partial \boldsymbol{\tau}}\right)^T\right] &= \frac{2}{M\sigma^2}\mathrm{Re}\left[\boldsymbol{A}^H(\boldsymbol{\tau})\boldsymbol{D}\boldsymbol{\alpha}\right],\\
E\left[\left(\frac{\partial \ln L}{\partial \mathrm{Im}(\boldsymbol{a})}\right)\left(\frac{\partial \ln L}{\partial \mathrm{Im}(\boldsymbol{a})}\right)^T\right] &= \frac{2}{M\sigma^2}\mathrm{Re}\left[\boldsymbol{A}^H(\boldsymbol{\tau})\boldsymbol{A}(\boldsymbol{\tau})\right],\\
E\left[\left(\frac{\partial \ln L}{\partial \mathrm{Re}(\boldsymbol{a})}\right)\left(\frac{\partial \ln L}{\partial \mathrm{Re}(\boldsymbol{a})}\right)^T\right] &= \frac{2}{M\sigma^2}\mathrm{Re}\left[\boldsymbol{A}^*(\boldsymbol{\tau})\boldsymbol{A}(\boldsymbol{\tau})\right],\\
E\left[\left(\frac{\partial \ln L}{\partial \boldsymbol{\tau}}\right)\left(\frac{\partial \ln L}{\partial \boldsymbol{\tau}}\right)^T\right] &= \frac{2}{M\sigma^2}\mathrm{Re}\left[\boldsymbol{\alpha}^H\boldsymbol{D}^H\boldsymbol{D}\boldsymbol{\alpha}\right],
\end{aligned}$$

here, $\boldsymbol{\alpha} = diag[a_1, \ldots, a_K]$, $\boldsymbol{D}$ is a complex matrix with dimensions $M \times K$, $\boldsymbol{D}_{(m,k)} = -jm\Delta\omega e^{-jm\tau_k\Delta\omega}R[m]$.

According to [32], the CRLB matrix for time delay estimation errors can be written as follows:

$$\mathrm{CRB}(\boldsymbol{\tau}) = \frac{M\sigma^2}{2}\left\{Re\left[\boldsymbol{\alpha}^H\boldsymbol{D}^H\left(\boldsymbol{I} - \boldsymbol{A}(\boldsymbol{\tau})\left(\boldsymbol{A}^H(\boldsymbol{\tau})\boldsymbol{A}(\boldsymbol{\tau})\right)^{-1}\boldsymbol{A}^H(\boldsymbol{\tau})\right)\boldsymbol{D}\boldsymbol{\alpha}\right]\right\}^{-1}. \quad (21)$$

Therefore, the lower bound of the time-delay estimation error $\mathrm{CRB}(\tau_i)$ for the i-th target is given by the i-th diagonal element of the CRLB matrix $\mathrm{CRB}(\boldsymbol{\tau})$, that is, $\mathrm{CRB}(\tau_i) = \mathrm{CRB}(\boldsymbol{\tau})[i, i]$. In this study, we define the total error bound of the time-delay estimation for multi-target as the sum of the CRLB of the time-delay estimation error for each target:

$$\mathrm{CRB}_\tau = \sum_{i=1}^{K}\mathrm{CRB}(\tau_i) = \mathrm{trace}(\mathrm{CRB}(\boldsymbol{\tau})). \quad (22)$$

V. SIMULATION EXPERIMENT

To validate the effectiveness of the proposed SR-ECD for multi-target time-delay estimation, we used LFM signals as reference signals and conducted Monte Carlo experiments to compare the output results of the SR-ECD (the SR-based estimation algorithm in the exponential correlation domain) with the SR-CD (the SR-based estimation algorithm in the correlation domain), as well as the classic MF-based estimation algorithm and the EF-based estimation algorithm. We also calculated the root mean squared errors (RMSE) of these estimation algorithms for multi-target time-delay estimation under different input SNR conditions and compared them with the error bound derived in (22).

The input SNR was calculated as $\mathrm{SNR}_{\mathrm{input}} = 10\lg\left(\sum_{m=1}^{M} r^2[m]/(M\sigma^2)\right)$. The RMSE of the time-delay estimation for multi-target is defined as:

$$\mathrm{RMSE}_{\boldsymbol{\tau}} = \sqrt{\frac{1}{J}\sum_{j=1}^{J}\left\|\hat{\boldsymbol{d}}_j - \bar{\boldsymbol{d}}\right\|_2^2} \quad (23)$$

where J is the number of Monte Carlo experiments. To facilitate error measurement, we assume that the true delay vector is a row vector $\bar{\boldsymbol{d}}$ of dimension M, where $\bar{\boldsymbol{d}}(m) = 1$ if and

$$\boldsymbol{A}(\boldsymbol{\tau}) = \begin{bmatrix} e^{-j\tau_1\Delta\omega}R[1] & e^{-j\tau_2\Delta\omega}R[1] & \cdots & e^{-j\tau_K\Delta\omega}R[1] \\ e^{-j2\tau_1\Delta\omega}R[2] & e^{-j2\tau_2\Delta\omega}R[2] & \cdots & e^{-j2\tau_K\Delta\omega}R[2] \\ \\ e^{-jM\tau_1\Delta\omega}R[M] & e^{-jM\tau_2\Delta\omega}R[M] & \cdots & e^{-jM\tau_K\Delta\omega}R[M] \end{bmatrix}_{M\times K}.$$

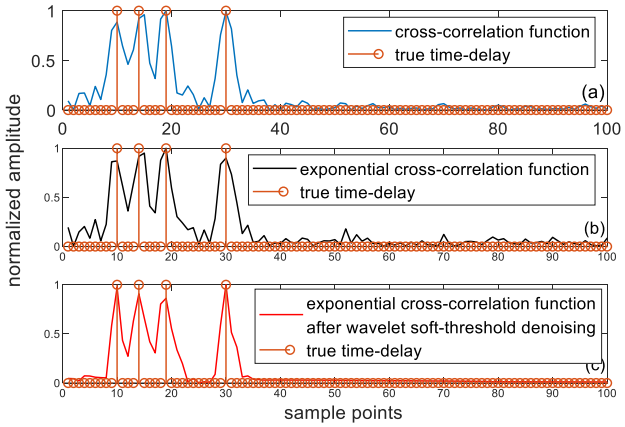

FIGURE 2. The output of the multi-target signal. (a) in correlation domain. (b) in exponential correlation domain. (c) the output in exponential correlation domain after wavelet soft threshold processing.

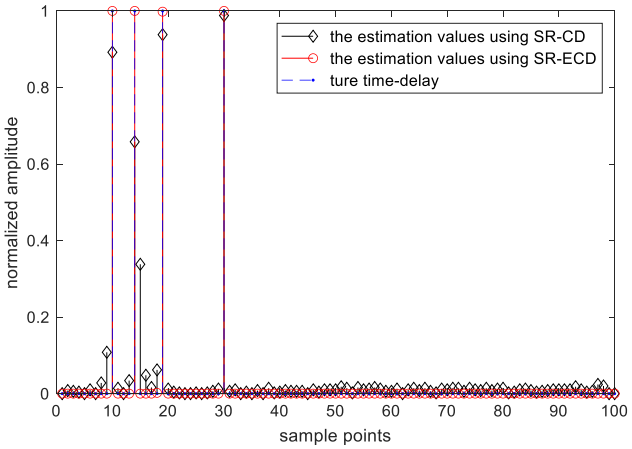

FIGURE 3. Multi-target time-delay estimation of SR-CD and SR-ECD.

only if $m = d_i, i = 1, 2, \ldots, K$, and all other $\bar{\boldsymbol{d}}(m) = 0$. The estimated delay vector given by the j-th Monte Carlo experiment for a corresponding algorithm is denoted by $\hat{\boldsymbol{d}}_j, j = 1, 2, \ldots, J$.

Experiment 1: The reference signal was an LFM signal with a bandwidth of 10MHz and a starting carrier frequency of 3000kHz. The total number of samples for the received signal containing the four targets was $L = 2000$, and the input SNR was -3dB. The true time-delays of the four targets were $d_1 = 10, d_2 = 14, d_3 = 19, d_4 = 30$ (in units of sample points). We set the EF output SNR threshold S_0 as α ($0 < \alpha \leq 1$) times the peak value of the MF output SNR, that is, the SNR threshold in the optimal exponent selection method is $S_0 = \alpha \max(\text{SNR}(p))$. When $\alpha = 0.95$, the optimal exponent provided by the method was $p_{opt} = -0.05$. Figure 2 shows the normalized output of the received signal after passing through the MF, EF with $p_{opt} = -0.05$, and EF with $p_{opt} = -0.05$ followed by wavelet soft-threshold denoising. It can be seen that the output of the EF in the exponential correlation domain (i.e., the exponential cross-correlation function) provides stronger resolution for multiple targets and has good noise immunity, resulting in more accurate time-delay estimation for multiple targets. In addition, the time delay estimation method based on the MUSIC algorithm is not suitable for this low SNR and adjacent target scenario and cannot provide an effective output for the four targets. Therefore, the proposed algorithm was not compared to the MUSIC algorithm in this study.

After performing $J = 500$ independent Monte Carlo experiments, the mean values of the estimated time-delays using SR-ECD ($p_{opt} = -0.05$) and SR-CD are presented in Figure 3. Combining Figure 2 and 3, it can be seen that compared to SR-CD (in the correlation domain), the SR-ECD (in the exponential correlation domain) proposed in this study has fewer spurious peaks and better resolution for multi-target. Therefore, the estimated time-delays using SR-ECD will be more accurate.

Experiment 2: Using the same received signal, reference signal, sampling rate, and grid number as in Simulation 1, we performed $J = 500$ independent Monte Carlo experiments to evaluate the RMSEs of the proposed SR-ECD, SR-CD, and classic MF- and EF- based time delay estimation algorithms at different input SNRs, as shown in Figure 4. Overall, the estimation accuracy of SR-ECD is significantly better than that of the MF- and EF- based time-delay estimation algorithms. Under the condition of an input SNR greater than -24dB, the proposed SR-ECD has a higher multi-target time-delay estimation accuracy than that of the SR-CD. This is because, for adjacent targets, the partial mutual coherence coefficient of the observation matrix in the proposed SR-ECD is lower, and the coherence between adjacent columns in the observation matrix is smaller, thereby improving the reconstruction performance of the delays of adjacent targets. Moreover, the estimation errors obtained by SR-ECD are closer to the error bound derived in (22) of the multi-target time-delay estimation. In addition, the corresponding RMSE curve of the proposed SR-ECD disappears on the right side when the input SNR is higher than -4dB. This is because at these input SNRs, the proposed SR-ECD directly solves for the exact time-delay estimate, and the logarithm of the error, which is zero, cannot be displayed. However, the results of SR-CD, and classic MF-based time delay estimation algorithms differ so much from the CRB. This is because the given targets are too close to each other, the resolution of these two algorithms is not sufficient to distinguish the corresponding targets.

Experiment 3: We used the same received and reference signals, sampling rate, and grid number as in simulation 1. We continue to analyze the effects of different parameters on the SR-ECD time delay estimation error. First, we set the grid number N to different values and the input SNR to 2.5dB, -3dB, and -15dB, respectively. We performed $J = 500$ independent Monte Carlo experiments to calculate the RMSEs of the time delay estimation for the proposed SR-ECD and SR-CD, as shown in Figure 5.

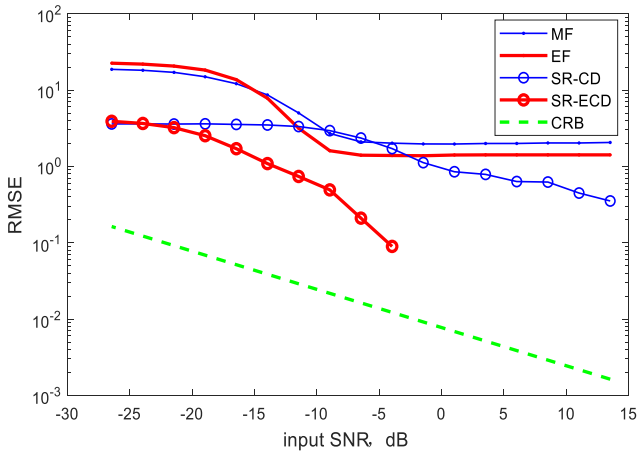

FIGURE 4. Estimation errors of four algorithms over the input SNR.

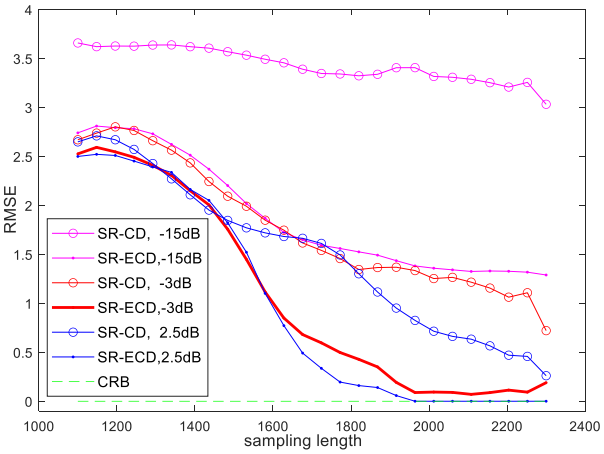

FIGURE 6. Under different input SNRs, estimation errors of SR-CD and SR-ECD over sampling length.

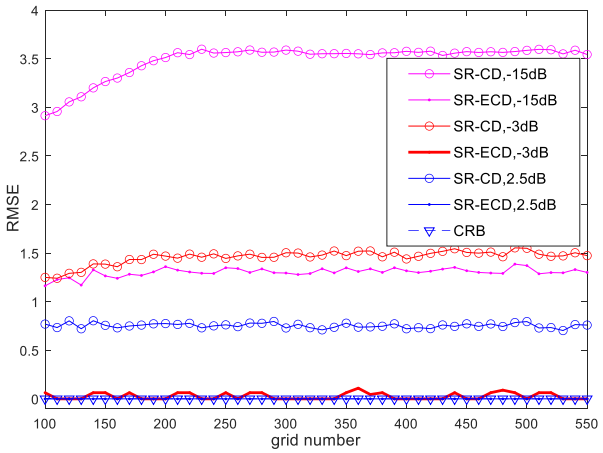

FIGURE 5. Under different input SNRs, estimation errors of SR-CD and SR-ECD over grid number.

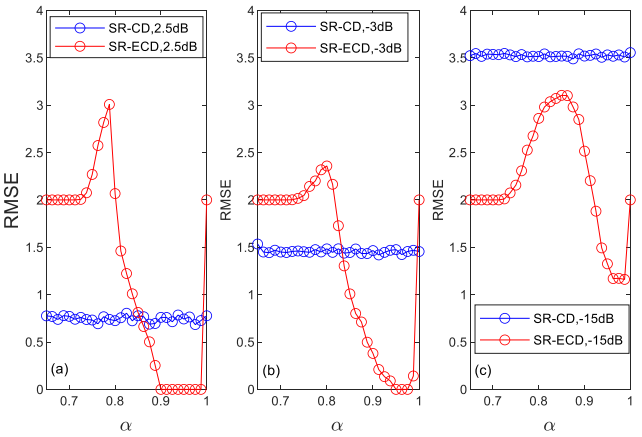

FIGURE 7. Estimation errors of SR-CD and SR-ECD over output SNR threshold α. (a) input SNR is 2.5dB. (b) input SNR is -3dB. (c) input SNR is -15dB.

It can be observed that under all three input SNR conditions, the time-delay estimation accuracy of the proposed SR-ECD is significantly higher than that of the SR-CD. Furthermore, as the SNR decreases, the estimation error increases considerably with an increase in grid number because of the increased partial mutual coherence coefficient of the observation matrix, as the number of column vectors in the observation matrix increases with an increase in grid number. However, when the SNR is relatively high, the algorithm has a stronger sparse reconstruction ability and is less sensitive to changes in the grid number within a certain range. At the same time, we also plotted the CRB with SNR $= 2.5$dB, where the CRB is a constant line under given noise variance, signal strength, and number of targets. It can be seen that, the estimation error of the proposed SR-ECD fits well with this CRB.

Next, for different sampling lengths L and input SNRs of 2.5 dB, -3 dB, and -15 dB, we performed $J = 500$ independent Monte Carlo experiments to calculate the RMSEs of the proposed SR-ECD and SR-CD for time-delay estimation, as shown in Figure 6. It can be observed that the RMSEs of both algorithms decrease as the sampling length L increases, with the error of SR-ECD showing a significantly faster reduction rate than that of SR-CD. When the sampling length L exceeds 2000, the estimation error of SR-ECD approaches a stable value. The estimation error of the proposed SR-ECD (with SNR $= 2.5$dB) also gradually approaches its corresponding CRB as the sampling length increases.

Finally, we investigate the effect of the proportion coefficient in the output SNR threshold α (0.5$\sim$1) on the time-delay estimation error of SR-ECD and SR-CD. The input SNRs were set to 2.5dB, -3dB, and -15dB, and the RMSE of the time delay estimation was calculated through $J = 500$ independent Monte Carlo experiments, as shown in Figure 7.

It can be observed that when α is less than a certain value, the time-delay estimation error curve of the SR-ECD does not show significant fluctuations. This is because when α is small, that is, the output SNR requirement is low, the controllable parameter p of EF can be set to its minimum value $p = -1$. Moreover, it can be observed that the range of achieving the minimum error decreased as the input SNR

decreased. Because the output SNR threshold is not set in SR-CD, its time-delay estimation error curve does not show fluctuations.

VI. CONCLUSION

In scenarios where multiple targets are closely spaced, the traditional time delay estimation algorithm based on the MF often suffers from the problem of main-lobe and side-lobe interference between targets, making it difficult to estimate the time delays of all targets accurately. The improved algorithm based on EF has a high resolution and can distinguish the time delays of different targets more accurately. However, EF is still susceptible to noise interference in low SNR scenarios, leading to inadequate accuracy in the time delay estimation.

Based on the output of EF (i.e., the exponential correlation function), this study constructed an SR model of the received signal in the exponential correlation domain. As shown, owing to the high resolution of the output of EF, the corresponding observation matrix of the proposed SR model has a smaller partial mutual coherence coefficient, which represents a higher reconstruction performance of the delays of adjacent targets. The interior-point method [26] is used to solve the proposed SR model. On the one hand, the method does not require prior knowledge of the number of targets and is suitable for high-dimensional data scenarios; on the other hand, it can remove the solution components below a certain threshold, which helps to filter out the noise and clutter to some extent and improves the estimation accuracy and stability of the algorithm in low SNR environments. The simulation results show that when the input SNR is higher than -24 dB, the proposed SR-ECD has a higher estimation accuracy for multi-target time delays (especially for adjacent targets) than MF, EF, and SR-CD. Particularly, when the input SNR is higher than -14 dB, the estimation error of SR-ECD is less than 1/3 of that of SR-CD and less than 1/5 of that of the traditional MF-based time-delay estimation algorithm, and its error is very close to the error bound of the multi-target time-delay estimation error. Moreover, when the input SNR is higher than -4 dB, it achieves completely accurate estimation.

In order to further improve the accuracy of time delay estimation of multiple targets, future research directions or potential challenges of the proposed algorithm may be algorithms using fewer observation data and more prior information, or algorithms combined with deep learning methods. Moreover, to have a wider scope of application, the proposed algorithm for joint estimation of time delay and direction of arrival parameters will be studied and compared with other algorithms.

REFERENCES

[1] L. Gaudio, M. Kobayashi, G. Caire, and G. Colavolpe, "On the effectiveness of OTFS for joint radar parameter estimation and communication," *IEEE Trans. Wireless Commun.*, vol. 19, no. 9, pp. 5951–5965, Sep. 2020.

[2] C. Zhang, W. Shi, Z. Gong, Q. Zhang, and C. Li, "Trajectory optimization for target localization using time delays and Doppler shifts in bistatic sonar-based Internet-of-Underwater-Things," *IEEE Internet Things J.*, vol. 10, no. 18, pp. 16427–16439, Sep. 2023.

[3] R. Shafin, L. Liu, Y. Li, A. Wang, and J. Zhang, "Angle and delay estimation for 3-D massive MIMO/FD-MIMO systems based on parametric channel modeling," *IEEE Trans. Wireless Commun.*, vol. 16, no. 8, pp. 5370–5383, Aug. 2017.

[4] W. Wang, T. Chen, R. Ding, G. Seco-Granados, L. You, and X. Gao, "Location-based timing advance estimation for 5G integrated LEO satellite communications," *IEEE Trans. Veh. Technol.*, vol. 70, no. 6, pp. 6002–6017, Jun. 2021.

[5] A. K. W. Chee, "Quantitative dopant profiling by energy filtering in the scanning electron microscope," *IEEE Trans. Device Mater. Rel.*, vol. 16, no. 2, pp. 138–148, Jun. 2016.

[6] G. Turin, "An introduction to matched filters," *IEEE Trans. Inf. Theory*, vol. IT-6, no. 3, pp. 311–329, Jun. 1960.

[7] A. H. Nitz, C. Capano, A. B. Nielsen, S. Reyes, R. White, D. A. Brown, and B. Krishnan, "1-OGC: The first open gravitational-wave catalog of binary mergers from analysis of public advanced LIGO data," *Astrophys. J.*, vol. 872, no. 2, p. 195, Feb. 2019.

[8] P. Willett, W. D. Blair, and X. Zhang, "The multitarget monopulse CRLB for matched filter samples," *IEEE Trans. Signal Process.*, vol. 55, no. 8, pp. 4183–4197, Aug. 2007.

[9] H. Chen, W. Wang, W. Liu, Y. Tian, and G. Wang, "An exact near-field model based localization for bistatic MIMO radar with COLD arrays," *IEEE Trans. Veh. Technol.*, early access, Jul. 12, 2023, doi: 10.1109/TVT.2023.3294625.

[10] Y. Yuan, Y. Luo, Y. Zhang, Z. Zhu, and J. Wang, "Design and implementation of multi-channel moving target radar signal simulator," *J. Eng.*, vol. 2019, no. 19, pp. 6081–6084, Jul. 2019.

[11] A. Liao, Z. Gao, H. Wang, S. Chen, M.-S. Alouini, and H. Yin, "Closed-loop sparse channel estimation for wideband millimeter-wave full-dimensional MIMO systems," *IEEE Trans. Commun.*, vol. 67, no. 12, pp. 8329–8345, Dec. 2019.

[12] M. Wang, F. Gao, S. Jin, and H. Lin, "An overview of enhanced massive MIMO with array signal processing techniques," *IEEE J. Sel. Topics Signal Process.*, vol. 13, no. 5, pp. 886–901, Sep. 2019.

[13] L. Liu and H. Liu, "Joint estimation of DOA and TDOA of multiple reflections in mobile communications," *IEEE Access*, vol. 4, pp. 3815–3823, 2016.

[14] Z. Zhang, F. Wen, J. Shi, J. He, and T.-K. Truong, "2D-DOA estimation for coherent signals via a polarized uniform rectangular array," *IEEE Signal Process. Lett.*, vol. 30, pp. 893–897, 2023.

[15] G. Zheng, Y. Song, Y. Liu, and G. Chen, "Search-free range and angle estimation for bistatic VHF-FDA-MIMO radar in complex terrain," *Signal Process.*, vol. 212, Nov. 2023, Art. no. 109163.

[16] G. Zheng, C. Chen, and Y. Song, "Height measurement for meter wave MIMO radar based on matrix pencil under complex terrain," *IEEE Trans. Veh. Technol.*, early access, Apr. 26, 2023, doi: 10.1109/TVT.2023.3268791.

[17] L. Zhang, K. Deng, H. Wang, and M. Luo, "Exponential filter-based delay estimation algorithm for active systems in the presence of multi-targets," *IET Radar, Sonar Navigat.*, vol. 7, no. 3, pp. 287–294, Mar. 2013.

[18] Z. Wan, Z. Gao, F. Gao, M. D. Renzo, and M.-S. Alouini, "Terahertz massive MIMO with holographic reconfigurable intelligent surfaces," *IEEE Trans. Commun.*, vol. 69, no. 7, pp. 4732–4750, Jul. 2021.

[19] X. Yuan, D. J. Brady, and A. K. Katsaggelos, "Snapshot compressive imaging: Theory, algorithms, and applications," *IEEE Signal Process. Mag.*, vol. 38, no. 2, pp. 65–88, Mar. 2021.

[20] V. Monga, Y. Li, and Y. C. Eldar, "Algorithm unrolling: Interpretable, efficient deep learning for signal and image processing," *IEEE Signal Process. Mag.*, vol. 38, no. 2, pp. 18–44, Mar. 2021.

[21] M. Rani, S. B. Dhok, and R. B. Deshmukh, "A systematic review of compressive sensing: Concepts, implementations and applications," *IEEE Access*, vol. 6, pp. 4875–4894, 2018.

[22] M. Lustig, D. Donoho, and J. M. Pauly, "Sparse MRI: The application of compressed sensing for rapid MR imaging," *Magn. Reson. Med.*, vol. 58, no. 6, pp. 1182–1195, Dec. 2007.

[23] F. Wang and X. Zhang, "Joint estimation of TOA and DOA in IR-UWB system using sparse representation framework," *ETRI J.*, vol. 36, no. 3, pp. 460–468, Jun. 2014.

[24] X. D. Leng, B. Ba, Z. Y. Lu, and D. M Wang, "Sparse reconstruction time delay estimation algorithm based on backtracking filter," *Acta Phys. Sin.*, vol. 65, no. 21, pp. 88–96, Mar. 2016.
[25] S. Wei, J. Peng, C. Tao, F. Wang, and D. Jiang, "A time delay estimation approach based on compressed sensing in dense multipath environmenta," in *Proc. IEEE Int. Conf. Inf. Autom. (ICIA)*, Jul. 2017, pp. 710–714.
[26] S.-J. Kim, K. Koh, M. Lustig, S. Boyd, and D. Gorinevsky, "An interior-point method for large-scale ℓ_1-regularized least squares," *IEEE J. Sel. Topics Signal Process.*, vol. 1, no. 4, pp. 606–617, Dec. 2007.
[27] S. G. Mallat, "Theory for multiresolution signal decomposition: The wavelet representation," *IEEE Trans. Pattern Anal. Mach. Intell.*, vol. 11, no. 7, pp. 674–693, Jul. 1989.
[28] J. Chen, X. Li, M. A. Mohamed, and T. Jin, "An adaptive matrix pencil algorithm based-wavelet soft-threshold denoising for analysis of low frequency oscillation in power systems," *IEEE Access*, vol. 8, pp. 7244–7255, 2020.
[29] S. Theodoridis, *Machine Learning: A Bayesian and Optimization Perspective*. Beijing, China: China Machine Press, 2017, pp. 424–431.
[30] S. G. Mallat and Z. Zhang, "Matching pursuits with time-frequency dictionaries," *IEEE Trans. Signal Process.*, vol. 41, no. 12, pp. 3397–3415, Dec. 1993.
[31] D. L. Donoho, M. Elad, and V. N. Temlyakov, "Stable recovery of sparse overcomplete representations in the presence of noise," *IEEE Trans. Inf. Theory*, vol. 52, no. 1, pp. 6–18, Jan. 2006.
[32] P. Stoica and A. Nehorai, "MUSIC, maximum likelihood, and Cramer–Rao bound," *IEEE Trans. Acoust., Speech, Signal Process.*, vol. 37, no. 5, pp. 720–741, May 1989.

LIN-FENG ZOU received the B.E. degree from Southwest Petroleum University, Chengdu, China. He is currently pursuing the M.S. degree with the College of Mathematics, Sichuan University. His research interests include signal processing, nonlinear dynamics, and application of intelligent systems.

YUN-FENG ZHU is currently pursuing the B.S. degree with the College of Mathematics, Sichuan University. His research interests include complex networks, parameter identification, and machine learning.

JIE GU received the B.S. and Ph.D. degrees in signal and information processing from the University of Electronic Science and Technology of China, Chengdu, China, in 1997 and 2004, respectively. His current research interests include adaptive array signal processing and mobile location in digital communication systems.

JING-FEI JIANG received the B.S. and M.S. degrees in electronic engineering from Fudan University, Shanghai, China, in 2008 and 2011, respectively. His main research interests include signal processing and its application for advanced sensors.

LU ZHANG received the B.S. degree in applied mathematics and the Ph.D. degree in mathematics from Sichuan University, Chengdu, China, in 2007 and 2012, respectively. She is currently an Associate Professor with the College of Mathematics, Sichuan University. Her current research interests include signal processing, statistical physics, and nonlinear dynamics.